



## AERYN: A simple standalone application for visualizing and enhancing elemental maps

Vincent Mouchi, Quentin G. Crowley, Teresa Ubide

### ► To cite this version:

Vincent Mouchi, Quentin G. Crowley, Teresa Ubide. AERYN: A simple standalone application for visualizing and enhancing elemental maps. *Applied Geochemistry*, 2016, 75, pp.44 - 53. 10.1016/j.apgeochem.2016.10.012 . hal-01393540

**HAL Id: hal-01393540**

**<https://hal.sorbonne-universite.fr/hal-01393540>**

Submitted on 7 Nov 2016

**HAL** is a multi-disciplinary open access archive for the deposit and dissemination of scientific research documents, whether they are published or not. The documents may come from teaching and research institutions in France or abroad, or from public or private research centers.

L'archive ouverte pluridisciplinaire **HAL**, est destinée au dépôt et à la diffusion de documents scientifiques de niveau recherche, publiés ou non, émanant des établissements d'enseignement et de recherche français ou étrangers, des laboratoires publics ou privés.

AERYN: a simple standalone application for visualizing and enhancing elemental maps

Vincent Mouchi<sup>\*1,2</sup>, Quentin G. Crowley<sup>1</sup> and Teresa Ubide<sup>1,3</sup>

<sup>1</sup>: Department of Geology, School of Natural Sciences, Trinity College Dublin, Museum Building,  
College Green, Dublin 2, Republic of Ireland

<sup>2</sup>: Current address: Sorbonne Universités, UPMC Univ. Paris 06, CNRS UMR 7193, IStEP, F-75005,  
Paris, France

<sup>3</sup>: Current address: The University of Queensland, Brisbane QLD 4072, Australia

\*: corresponding author: vmouchi@gmail.com

## Abstract

Interpretation of high spatial resolution elemental mineral maps can be hindered by high frequency fluctuations, as well as by strong naturally-occurring or analytically-induced variations. We have developed a new standalone program named AERYN (Aspect Enhancement by Removing Yielded Noise) to produce more reliable element distribution maps from previously reduced geochemical data. The program is Matlab-based, designed with a graphic user interface and is capable of rapidly generating elemental maps from data acquired by a range of analytical techniques. A visual interface aids selection of appropriate outlier rejection and drift-correction parameters, thereby facilitating recognition of subtle elemental fluctuations which may otherwise be obscured. Examples of use are provided for quantitative trace element maps acquired using both laser ablation (LA-) ICP-MS and electron probe microanalysis (EPMA) of the cold-water coral *Lophelia pertusa*. We demonstrate how AERYN allows recognition of high frequency elemental fluctuations, including those which occur perpendicular to the maximum concentration gradient. Such data treatment compliments commonly used processing methods to provide greater flexibility and control in producing elemental maps from micro-analytical techniques.

Keywords: LA-ICP-MS; EDS; WDS; element distribution maps; processing; Matlab; biominerals.

## 1. Introduction

Element distribution maps or images acquired using in-situ analytical techniques are widely used in Geology and Earth Sciences (e.g. Cusack et al., 2008; Rittner & Müller, 2012; McGowan et al., 2014).

Several software packages exist to process element distribution maps (Paul et al., 2012; Rittner & Müller, 2012; Ortolano et al., 2014), with some recent studies having investigated multi-trace element maps processed from data obtained by laser ablation inductively coupled plasma mass spectrometry (LA-ICP-MS) (e.g. Petrus & Kamber, 2013; Paul et al., 2014; Ubide et al., 2015).

Common issues in micro-analytical techniques linked to data acquisition, such as analytical drift and outliers, can greatly influence the quality of resultant elemental maps. We propose a user-friendly method created using the programming software Matlab (MathWorks; <http://www.mathworks.com/products/matlab>) to deconvolute complex data and produce more readable elemental maps. LA-ICP-MS data must have been previously reduced to account for baseline correction and reference material calibration, e.g. by using common data reduction software. Our program, which we term AERYN (Aspect Enhancement by Removing Yielded Noise), allows the filtering of outliers and smoothing of values included in a data matrix, resulting in an increased readability and importantly permitting more representative and accurate interpretation of heterogeneity in elemental distribution. In addition, we propose a de-trending option to highlight subtle geochemical features which may be obscured by strong signal fluctuations, either natural in origin or caused by instrumental drift. AERYN has been compiled and exported as a standalone application for Windows, allowing its use on a PC without the requirement of a Matlab licence (<http://www.tcd.ie/Geology/staff/crowleyq/AERYN/>). The only requirement for this program to perform correctly is to download and install the free Matlab Runtime R2015a (8.5) from the MathWorks website (<http://www.mathworks.com/products/compiler/mcr>).

To illustrate how AERYN operates, we present elemental maps acquired by LA-ICP-MS and electron probe microanalysis (EPMA) from the wall of the skeleton of the cold-water coral *Lophelia pertusa*. Virtually any type of numeric compositional map can use part or all of the protocol described here, as

long as the data fit to a square or rectangular shape (in laser-based systems, this can be achieved by analysing either parallel equivalent line scans or a grid of regularly-spaced spots). We provide the corresponding Matlab code and the standalone application as well as a "Read Me" file with some specifications as supplementary material, allowing the software to be adapted by other users.

## 2. AERYN description

### 2.1 User interface

AERYN is presented with a control panel on the left-hand side and three graphic areas on the right-hand side (Fig. 1). The upper graphic displays an elemental map (using Matlab's "imagesc" function) whereas the lower-left graphic displays a 3-dimensional view of the data (using Matlab's "surf" function). The lower-right graph represents a histogram of the data (number of bins calculated using Yule's rule) to graphically illustrate the distribution of elemental concentration represented in the other graphic displays.

### 2.2 Importing data

AERYN uses text files (.txt, .tsv) exported from a variety of elemental map processing software or from Microsoft Excel. We tested exports from LA-ICP-MS, Scanning Electron Microscopy with electron-dispersive spectroscopy (SEM-EDS) and EPMA maps, but text files from any software should be compatible. If not, we advise the user to follow instructions provided in the "Read Me" file.

AERYN does not process raw data, and a preceding data reduction step is still required. We used Iolite (Paton et al., 2011; v. 2.5 and 3.0) for data reduction prior to importing in AERYN. To import the numeric matrix corresponding to the map file, AERYN passes any number of lines composed of characters and reads only the part of the file containing the concentration values. The size of the imported matrix is only restricted by computer performance for very large datasets.

Once a numeric matrix has been generated, it is automatically displayed as a map on the upper graph and as a 3D surface plot of the 2D data on the lower-left graph (Fig. 1). It is therefore possible to rotate the lower-left graph or to automatically orient the view to a side section, in order to have better visibility of outliers and fluctuations. Moreover, if required for better display, it is possible to

transpose the matrix by clicking on "Transpose" in order to invert lines with columns.

From this point and at any stage, the user can cancel any number of operations made on the data by clicking on the "Undo" button.

### 2.3 Outlier removal

Outliers can be either extremely high or low values in comparison to the rest of the observed data and introduce bias in interpretations. AERYN allows the user to locate and remove all outliers at once. All removed outliers are replaced by empty spaces in the matrix (NaN). Processing of these spaces is explained in the following section. A statistical test is proposed to the user to define automatic thresholds of outliers based on the following equations (Tukey, 1977; Carling, 2000):

$$(1) \text{ Tup} = P90 + 1.5 * \text{IQR}$$

$$(2) \text{ Tdown} = P10 - 1.5 * \text{IQR}$$

With P90 the percentile at 0.90 for the dataset, P10 the percentile at 0.10 and  $\text{IQR} = P90 - P10$ . All values not occurring within the interval between Tdown and Tup are considered as dataset outliers. Such a statistical treatment will likely be sufficient for most datasets, though for the data presented here the cut is too drastic and the upper end of some high value areas is lost, preventing an accurate reading of the corresponding concentrations. For this reason, a second technique, based on iterative visual definition of outliers, is made available for the user.

Firstly, for the high value outliers, it is necessary to estimate the upper limit of data to be retained. For this, the "surf" function of Matlab is extremely powerful. By displaying the elemental map in 3D on the lower-left graph (with the concentrations in the z axis) and with the possibility of rotating the image, one can clearly (i) identify variations in concentration, (ii) assess the potential presence of trends that would require a correction at a later stage, and (iii) identify obvious outliers and their approximate values. At this stage, successive outlier removal steps can be achieved by searching for values in the dataset lower or higher than a chosen specific value (Fig. 2). Moreover, the histogram on the third graph (lower-right area) allows a better estimate of the minimum and maximum values to be chosen for the colour palette in order to highlight most of the compositional information.

Spatially-restricted high concentration areas are maintained as a whole with this method, though more

subjectively compared to the automatic definition of outliers as presented above. It should be noted that a possibility of inadvertently “over-trimming” the dataset exists, especially when controlled by the user, and therefore outlier removal should be done with caution (e.g., Fig. 2c).

For the second phase of outlier removal, a lower minimum limit value expected for quantitative or semi-quantitative data is zero. This minimum value can be higher if the concentrations of the studied elements are high, but in the present example the concentrations are low and can easily be cut to positive values without further consideration. If the mapped area is not entirely filled with sample material (i.e., if a sample was mounted in epoxy resin and this resin was intentionally ablated in order to obtain a rectangular map), the user must ensure that the resin value, which is generally constant, is still included in the data to prevent incorrect resampling of these areas by the outlier removal step.

This step can have multiple iterations as successive outlier removals allow an improved visualisation of geochemical fluctuations. The automatic Side View is extremely valuable at this stage as the outlier values as well as the signal to be retained are indicated by the vertical axis. During the whole process however it is necessary to keep in mind that some valuable geochemical information can reside in high-frequency variability. It is thus unwise to crop the highest or lowest values too close to the main visible fluctuations (see Fig. 2a and caption). Moreover, one must be aware that the larger the holes caused by outlier removal, the less accurate the following steps will become. We suggest that the number of outliers compared to the size of the data must be reasonably low. As an indication, the number of points removed in Figure 2 represent approximately 0.5 % of the dataset (see Fig. 2c).

Each time the user filters the dataset, a temporary message is displayed in the history box to indicate the percentage of data cropped compared from the entire matrix. The cut values are displayed on the map as white areas. Once outlier removal has been validated, the side view and the histogram can provide preliminary boundaries for the colour palette (Fig. 2b). The filters can be cancelled to retain the entire initial dataset while maintaining the palette range values.

#### 2.4 Filling gaps following outlier removal

In the outlier removal step, the outliers have been automatically replaced by the specific passive value NaN. The "inpaint\_nans" function (D'Errico, 2004) allows replacement of NaNs by analyzing

surrounding values for interpolation and extrapolation. With this step completed, the maps are efficiently “cleaned” of outliers.

This gap-filling step should not be performed after further steps such as smoothing, as the method used here substantially increases the number of NaN values in direct connection to pre-existing NaN values. For this reason, we chose to automatically fill the NaNs at the validation of the outlier removal.

## 2.5 Smoothing

An option to perform median filtering is available at this stage of data correction. Numerous smoothing functions and methods are available in the Matlab environment. In order to take into account the possible variability present on both x and y axes, the "medfilt2" function was chosen. This function calculates the mean of all values included in a moving square centred on a value to smooth, in order to replace that value with the mean, before moving the mask to the adjacent value. A larger mask results in a stronger applied smoothing function. If the dataset presents a strong background noise, it may be valid to repeat this step a second time, but it should be noted that if this option is performed, absolute values of concentration will not be accurate. The mean will be identical, but the absolute values of the extremes will no longer correspond to those given by initial data reduction and the map will therefore be semiquantitative. Relative fluctuations, however, will remain the same.

## 2.6 Detrending

The detrending option is useful in two different scenarios. Firstly, if a strong naturally-occurring trend is measured in the sample, the colour palette (commonly used to present fluctuation patterns) will only show this particular trend. Any higher frequency fluctuations along this trend or variations orthogonal to this direction (commonly observed in biominerals due to non-linear growth) and/or fluctuations of lower amplitude are thus invisible. Removing this main trend will allow qualitative study of such fluctuations. Additionally, if the background noise or sensitivity gradient is skewed as a result of experimental drift, a correction must be applied to stabilize the response across the elemental image. The technique presented here makes it possible to use data, even when a dramatic instrumental

drift occurs during an analytical session.

As is the case for smoothing, the process of detrending may change absolute values, so any interpretations can only be proposed for elemental distribution and relative fluctuations in concentration, in a semiquantitative fashion. Even in the case of naturally occurring trends, this option allows observation of lateral variations in concentrations that would otherwise be concealed.

The particular data set presented here shows a general trend of a supposedly decrease in Sr all along acquisition time, with data acquisition progressing in successive lines from left to right then top to bottom.

A first option to deal with this trend is to execute an automatic detrending. By clicking the corresponding button, AERYN calculates the best fitting linear plane to the data and applies a detrending corresponding to this plane.

Alternatively, to improve visibility in this case we can select a transect representative of the main fluctuation. By calculating the equation of the linear trend of this transect, it is possible to apply this equation as a correction to all lines (or columns) and reveal geochemical fluctuations across the entire map (Fig. 3). With this simple operation and even in the case of instrumental drift, it is possible to work on the map without necessarily having to return to data acquisition.

When selecting a line or a column and clicking on "Display", two new windows present the selected transect and its calculated linear trend on one panel (Fig. 3a), and the same transect along with its detrended transect on the other (Fig. 3b). No operations to the map have been done at this stage. If satisfied with these detrending parameters, the user can close both computer windows and Validate. This will detrend the matrix and display the detrended map on all graphs (Fig. 3c). If the calculated transects are not satisfactory, they can be cancelled by resetting the detrending operation.

The corrected map now presents fluctuations in Sr which are visible as coherent bands both at the top and bottom of the map, showing continuity of these features. The map can be smoothed to clean the high-frequency fluctuations using a 5x5 mask (Fig. 4).

## 2.7 Export map

At any stage, it is possible to export the matrix. In order to maintain optimum picture quality, the



maps are exported as TIFF files without compression with a uniform size of both dimensions of the map. The user is asked to enter the path and file names. The matrix itself and the historic record of operations made are saved as tab delimited text files, and the data are subsequently importable in AERYN for further modification if required.

Figure 5 presents the Sr map used as an example here as well as a Li map from the same acquisition session after data reduction (Iolite v. 3.0) and after post-processing using AERYN. Whereas maps processed only with data reduction software are noisy and hamper visibility of concentration bands, these bands are clearly visible after processing with AERYN. If required, in order to counteract the standardization of the dimension of the map after saving with AERYN, it is possible to import the TIFF file in another image software (e.g., Adobe Photoshop) to resize the image to the proper aspect ratio.

### 3. Example materials

Specimens of the cold water coral *L. pertusa* were prepared at Trinity College Dublin using the protocols described in Mouchi et al. (2014). Cleaned aragonitic skeletons were embedded in epoxy resin and cut longitudinally with a Buehler Isomet Low Speed Saw. Sections obtained were polished and subsequently etched with 2 % formic acid for 50 s. The etching protocol allowed direct acquisition of measurements on LA-ICP-MS without pre-ablation.

#### 3.1 LA-ICP-MS

Geochemical data were collected using an Analyte Excite 193 nm excimer ArF\* laser ablation system (Photon-Machines Inc.) coupled to an iCAP-Q ICP-MS unit (Thermo Scientific) at the Trinity College Dublin geochemistry facility. Details on the instrument setup for elemental mapping can be found in Ubide et al. (2015). Parallel and slightly overlapping (1  $\mu\text{m}$ ) line scans were acquired as suggested by Ubide et al. (2015) to avoid gaps during data acquisition without notable contamination from adjacent lines. A square beam of 12  $\mu\text{m}$  was selected with 10 Hz repetition rate at 8  $\mu\text{m.s}^{-1}$  scan speed and a laser fluence of 3.9 J.cm<sup>-2</sup>. Ion intensities of <sup>7</sup>Li, <sup>43</sup>Ca, <sup>86</sup>Sr and other isotopes not discussed here were measured for a total dwell time of 146 milliseconds. Individual dwell times were

225 70 ms for  $^7\text{Li}$ , 5 ms for  $^{86}\text{Sr}$  and 10 ms for  $^{43}\text{Ca}$ . Data acquisition procedures ran for a total of 2.5 h.  
 226 Either NIST SRM 610 or NIST SRM 612 was ablated for approximately 120 s using the same  
 227 ablation parameters as the unknown line scans. Two calibration lines were used at the beginning and  
 228 end of each experiment and one additional line every 10 unknown sample lines which equates to 120 s  
 229 of data acquisition on the reference material every approximately 25 minutes. Collected data were  
 230 then processed for quantitative values with the Iolite software (Paton et al., 2011; v. 2.5 and 3.0) using  
 231 the Trace\_Elements data reduction scheme (included in the Iolite program package) and the recently  
 232 accepted values of NIST SRM 610 and NIST SRM 612 (Jochum et al., 2011).  $^{43}\text{Ca}$  was used as the  
 233 internal standard, assuming a stoichiometric Ca content. Reduced data were then exported to be  
 234 readable and further treated by AERYN; instructions to export text files readable by AERYN from  
 235 Iolite are in the "Read Me" file provided as supplementary material.  
 236 Depending on the size of the acquisition area for each specimen, typical maps have between 950 and  
 237 1950 columns for 30 to 60 lines, corresponding to approximately 1-2 mm by 330-660  $\mu\text{m}$ ,  
 238 respectively.  
 239 The description of AERYN presented above (Fig. 1-5) used the map of distribution of Sr in *L. pertusa*  
 240 as example. The map of distribution of Li (Fig. 6a) does not require the outlier removal step as the  
 241 Side View indicates that the majority of measured fluctuations are below the resin value (see the  
 242 arrows on Fig. 6a) and visible. Indeed, though some positive outliers are present on the right-hand  
 243 side, they do not prevent reading of the minimum and maximum values on the histogram for palette  
 244 definition. The map is however difficult to interpret in terms of the location of fluctuations in Li  
 245 concentrations. The top part of the map is depleted in Li, as indicated by blue areas in opposition to  
 246 red and yellow areas on the lower part of the map. An automatic detrending applied to reduce the  
 247 amplitude of the fluctuations from top to bottom (Fig. 6b) aids in the visualization of several areas of  
 248 higher and lower Li concentration oriented N-S in this view.  
 249 From this step, a light smoothing using a 3 by 3 points mask further highlights the fluctuations. A  
 250 wider mask was not chosen due to the reduced number of lines in this map (only 30). Except for the  
 251 high value areas (in red) on the rightmost part of the map, both the map and the Side View show  
 252 higher amplitudes of fluctuations on the left-hand part compared to the right-hand part of the map

(Fig. 7). As this side of the coral skeleton displaying elevated elemental concentrations corresponds to the initial stage of skeletal growth, this map can be interpreted in terms of environmental forcing or kinetic incorporation, as suggested by Mouchi et al. (2014) from a simple transect (i.e. the elemental variation of Li shown here is real and not an analytical or data processing artefact).

### 3.2 Electron microprobe

Another *L. pertusa* specimen was mapped with a Cameca SX-*Five* electron microprobe at the Camparis Service, Paris, France. Acquisition parameters were 15 keV, 200 nA, 500 ms dwell time per point with a 4  $\mu\text{m}$  beam diameter and step size on a surface of 580 by 1352  $\mu\text{m}$ . The map presented here corresponds to Mg wt% (Fig. 8) after calibration using internal reference materials for each measurement. The analytical uncertainty for this element using this protocol is approximately 100  $\mu\text{g.g}^{-1}$  (2 SD).

Although a dwell time of 500 ms was used for this analytical protocol, which is high compared to common trace element mapping protocols (usually set at around 300 ms), fluctuations in Mg concentrations are still difficult to observe (Fig. 8a) and seem to be lower than the 100  $\mu\text{g.g}^{-1}$  uncertainty. The visibility of these subtle fluctuations in Mg concentration can be improved using AERYN (Fig. 8b).

The corresponding export files were written with transposed matrices compared to the ones generated by Iolite. The "Transpose" button in AERYN was used to get the same orientation as for the LA-ICP-MS maps. After filtering the data to cut the outliers, the map remains very noisy due to low concentration values. We applied a 7x7 mask to strongly reduce the high-frequency fluctuations and applied a weak detrending as the first lines presented lower values. The resulting map is shown in Figure 8b.

The limits of the bands of high and low concentrations remain difficult to establish, but AERYN permits areas of lower concentrations within high concentration bands to be more clearly visualized, in particular around columns number 40, 80, 170 and 225. The map is therefore ready for interpretation. High concentration bands are wider on the left-hand side (corresponding to the initial

stages of skeletal growth) than on the right-hand side of the map. Whereas a detailed interpretation of the geochemical variations presented in these maps is beyond the scope of this paper, if Mg incorporation is, as Sr incorporation, governed by kinetics in the skeleton of *L. pertusa*, this observation would indicate in the present dataset that early stages of skeletal growth may feature enhanced growth fluctuations. The large bands of high Mg concentration also tend to indicate that most of these early stages present high growth rates and that the low growth rate periods are temporally extremely restricted. These observations are in accordance of those of Mouchi et al. (2014) and Rollion-Bard & Blamart (2015).

#### 4. Conclusion

AERYN uses data generated from micro-analytical techniques and processed by data reduction software (such as Iolite) to improve the interpretation of elemental distribution maps. This paper has presented an alternative way to the trial-and-error routine of modification of palette thresholds by allowing the user to display the geochemical dataset in 3D and observe data extremes systematically. Moreover, AERYN allows the user to counteract any apparent changes due to instrumental drift, which might not be possible to correct with traditional data reduction schemes. AERYN makes it possible to observe discrete areas of high or low concentration which may be hidden by natural strong fluctuations or analytical artefacts. This program can highlight subtle variations in elemental maps in just a couple of minutes, thereby enhancing the interpretation of elemental maps obtained with a variety of analytical techniques such as LA-ICP-MS, EPMA and SEM-EDS.

#### Acknowledgements

The work presented in this paper was made possible by the ENS Ph.D. programme. The Earth and Natural Sciences Doctoral Studies Programme is funded under the Programme for Research in Third-Level Institutions Cycle-5 and co-funded under the European Regional Development Fund. The authors would like to thank Cora McKenna for her help operating the LA-ICP-MS, and Eric P. Verrecchia for his advice on some algorithms for the code of AERYN. John D'Errico kindly offered

the use of his Matlab function `inpaint_nans`. We acknowledge detailed feedback from one reviewer and the editor which helped us improve the original version of the manuscript.

## References

- Carling, K., 2000. Resistant outlier rules and the non-Gaussian case. *Comput. Stat. Data. An.* 33, 249-258.
- Cusack, M., Dauphin, Y., Cuif, J.-P., Salomé, M., Freer, A., Yin, H., 2008. Micro-XANES mapping of sulfur and its association with magnesium and phosphorus in the shell of the brachiopod, *Terebratulina retusa*. *Chem. Geol.* 253, 172-179.
- D'Errico, J., 2004. `inpaint_nans`. MATLAB Central File Exchange. Retrieved October, 20, 2014.
- Jochum, K.P., Weis, U., Stoll, B., Kuzmin, D., Yang, Q., Raczek, I., Jacob, D.E., Stracke, A., Birbaum, K., Frick, D.A., Günther, D., Enzweiler, J., 2011. Determination of reference values for NIST SRM 610-617 glasses following ISO guidelines. *Geostand. Geoanal. Res.* 35, 397-429.
- McGowan, N., Fowler, A.M., Parkinson, K., Bishop, D.P., Ganio, K., Doble, P.A., Booth, D.J., Hare, D.J., 2014. Beyond the transect: An alternative microchemical imaging method for fine scale analysis of trace elements in fish otoliths during early life. *Sci. Total Environ.* 494-495, 177-186.
- Mouchi, V., Crowley, Q.G., Jackson, A.L., McDermott, F., Monteys, X., de Rafélis, M., Rueda, J.L., Lartaud, F., 2014. Potential seasonal calibration for palaeoenvironmental reconstruction using skeletal microstructures and strontium measurements from the cold-water coral *Lophelia pertusa*. *J. Quaternary Sci.* 29, 803-814.
- Ortolano, G., Zappalà, L., Mazzoleni, P., 2014. X-Ray Map Analyzer: A new ArcGIS based tool for the quantitative statistical data handling of X-ray maps (Geo- and material-science applications). *Comput. Geosci.* 72, 49-64.
- Paton, C., Hellstrom, J., Paul, B., Woodhead, J., Hergt, J., 2011. Iolite: Freeware for the visualisation and processing of mass spectrometric data. *J. Anal. Atom. Spectrom.* 26, 2508-2518.
- Paul, B., Paton, C., Norris, A., Woodhead, J., Hellstrom, J., Hergt, J., Greig, A., 2012. CellSpace: A module for creating spatially registered laser ablation images within the Iolite freeware environment. *J. Anal. Atom. Spectrom.* 27, 700-706.

337 Paul, B., Woodhead, J.D., Paton, C., Hergt, J.M., Hellstrom, J., Norris, C.A., 2014. Towards a method  
 338 for quantitative LA-ICP-MS imaging of multi-phase assemblages: mineral identification and analysis  
 339 correction procedures. *Geostand. Geoanal. Res.* 38, 253-263.  
 340 Petrus, J.A., Kamber, B.S., 2013. A novel 2D LA-ICP-MS data analysis and visualization solution.  
 341 *Goldschmidt2013 Conference Abstracts*, 1959.  
 342 Rittner, M., Müller, W., 2012. 2D mapping of LA-ICPMS trace element distributions using R.  
 343 *Comput. Geosci.* 42, 152-161.  
 344 Rollion-Bard, C., Blamart, D., 2015. Possible controls on Li, Na, and Mg incorporation into aragonite  
 345 coral skeletons. *Chem. Geol.* 396, 98-111.  
 346 Tukey, J.W., 1977. *Exploratory Data Analysis*. Addison Wesley, Pennsylvania.  
 347 Ubide, T., McKenna, C.A., Chew, D.M., Kamber, B.S., 2015. High-resolution LA-ICP-MS trace  
 348 element mapping of igneous minerals: in search of magma histories. *Chem. Geol.* 409, 157-168, doi:  
 349 10.1016/j.chemgeo.2015.05.020.  
 350

### **Figure captions**

Figure 1: Main window of AERYN showing a Sr distribution map measured by LA-ICP-MS on a *Lophelia pertusa* specimen. Data were reduced in terms of baseline correction and standard calibration prior importation in AERYN. At this stage, no corrections have been applied.

Figure 2: Coral skeleton Sr content measured by LA-ICP-MS as line scans at the outlier removal step (colour bar represents concentration in  $\mu\text{g.g}^{-1}$ ) using Matlab's "surf" function. a: Map after filtering data out below 0 and above  $100,000 \mu\text{g.g}^{-1}$ . b: Side view rotated to expose the surface, showing the areas with the cut values in white (located by the arrows). c: Side view once the filtering has been validated. In order to retain the representative variability in the dataset, we advise not to cut the outliers below the values indicated here by the embedded red dashed line below which fluctuations do not appear anymore as discrete outliers. d: Final map and side view after removing outliers above  $20,000 \mu\text{g.g}^{-1}$  (corresponding to the red dashed line in c). At this stage, the histogram distribution can help to define the range for the colour palette (red dashed lines). The high count bin around  $0.6 \cdot 10^4 \mu\text{g.g}^{-1}$  corresponds to the resin value (i.e. not the biogenic carbonate) and is represented in dark blue on both sides of the map.

Figure 3: Detrending applied to the Sr distribution map. a: Selected transect from the map (in black) and calculated trend (in red). b: The original transect (black) and the detrended transect (red). c: Map after outlier removal and prior detrending is applied (compare to Fig. 2). d: Graphs obtained after detrending and rescaling palette range.

Figure 4: Sr distribution map after automatic detrending and smoothing with a 5 by 5 mask.

Figure 5: Element distribution maps resulting from data reduction using Iolite v. 3.0 (left) and after processing by AERYN (right) for Sr (a) and Li (b). Concentration bands are more clearly visible after processing with AERYN.

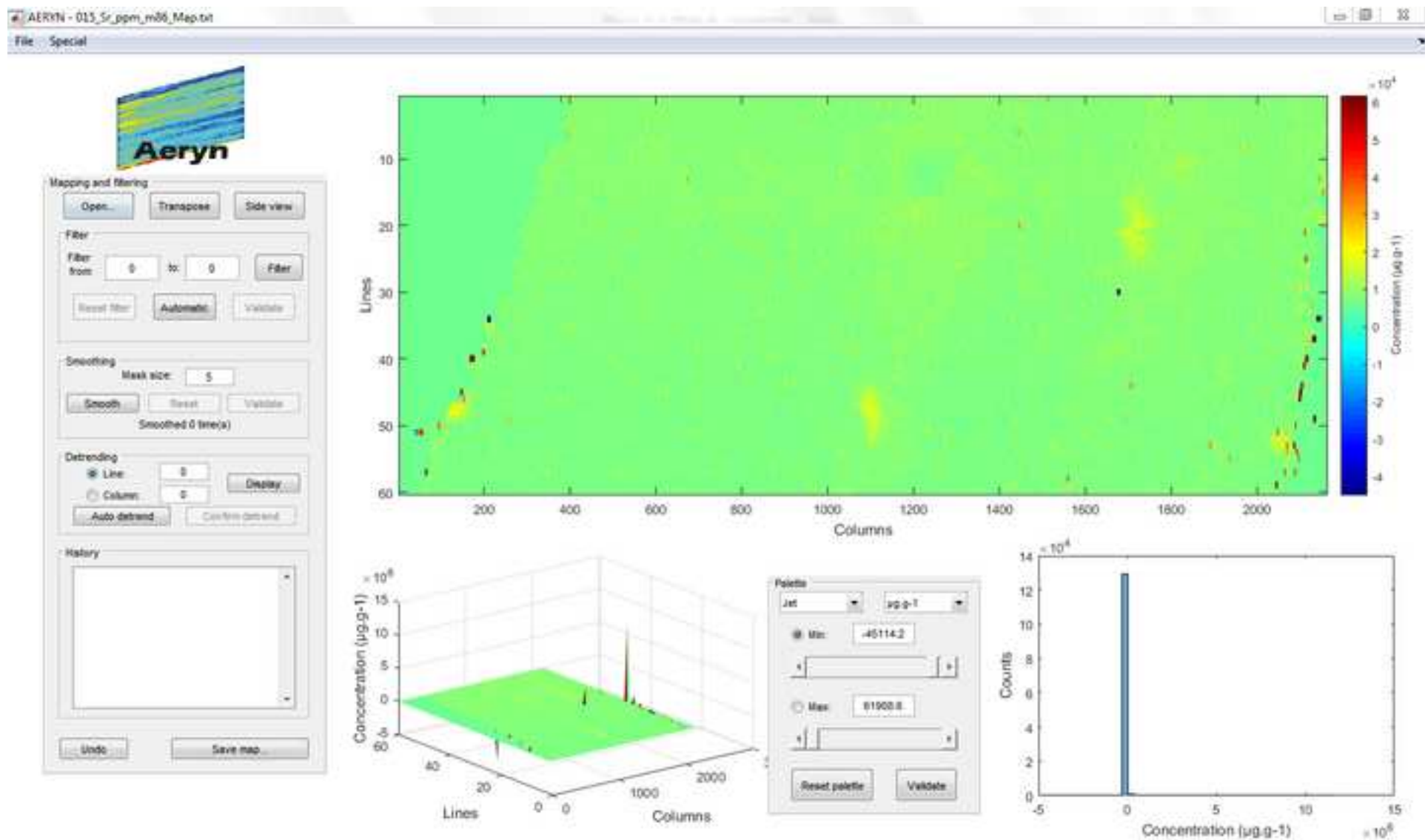
Figure 6: First steps for the Li map. a: Initial data after import of the Iolite export file. The resin is indicated by the arrows on the map and the Side View. b: Map after automatic detrending.

Figure 7: Smoothed map of Li concentration, using a 3x3 mask (each value replaced by the mean of all surrounding values in a 3 by 3 points area). Skeletal growth direction is right to left on this map.

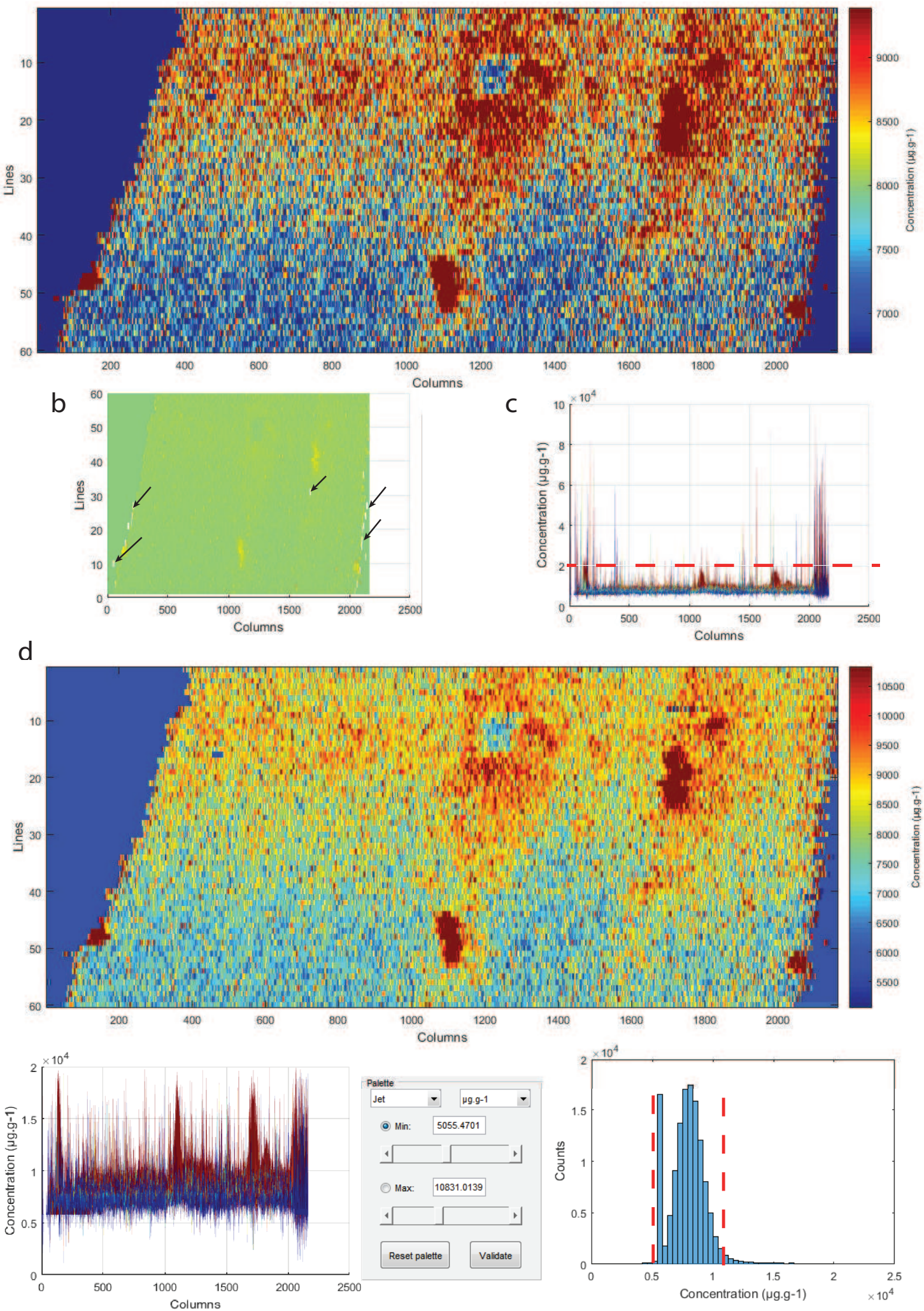
Figure 8: Mg (wt.%) map of a *L. pertusa* specimen acquired by electron microprobe, as obtained by the SX acquisition software (a) and after processing with AERYN by smoothing using a 7x7 mask and detrending (b). Skeletal growth direction is left to right on this map.



**Figure 1**  
[Click here to download high resolution image](#)



**Figure 2**





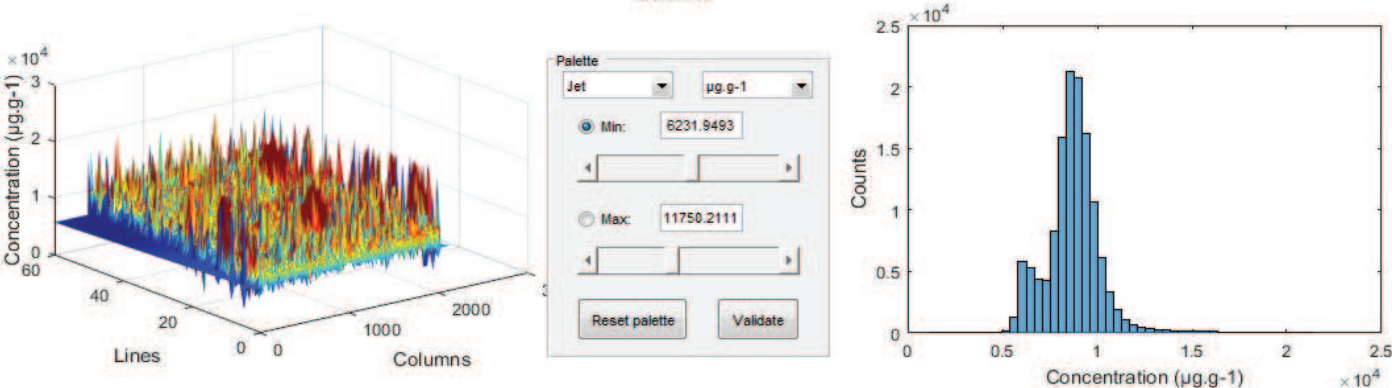
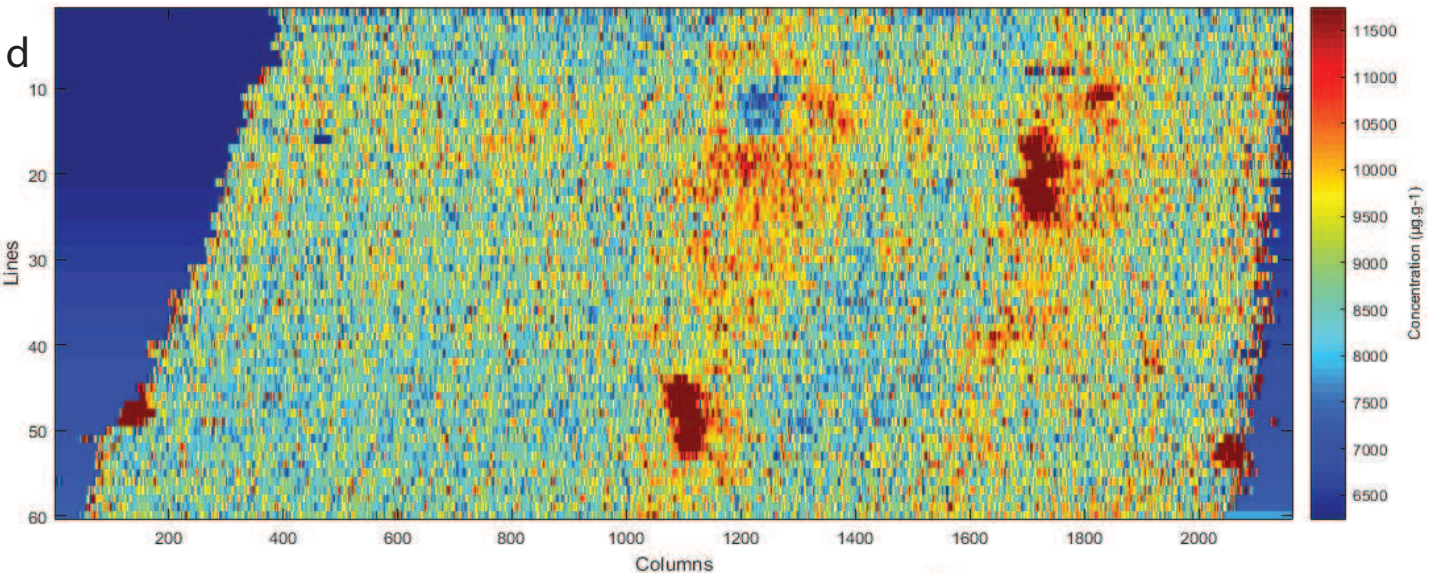
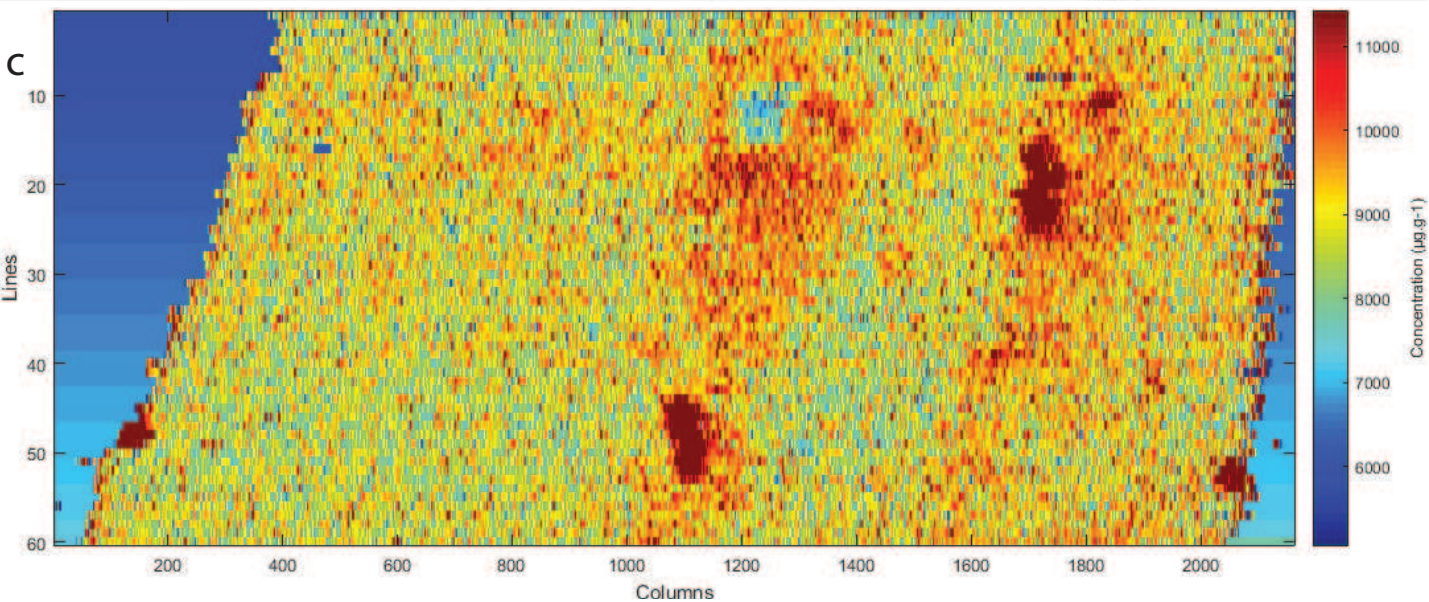
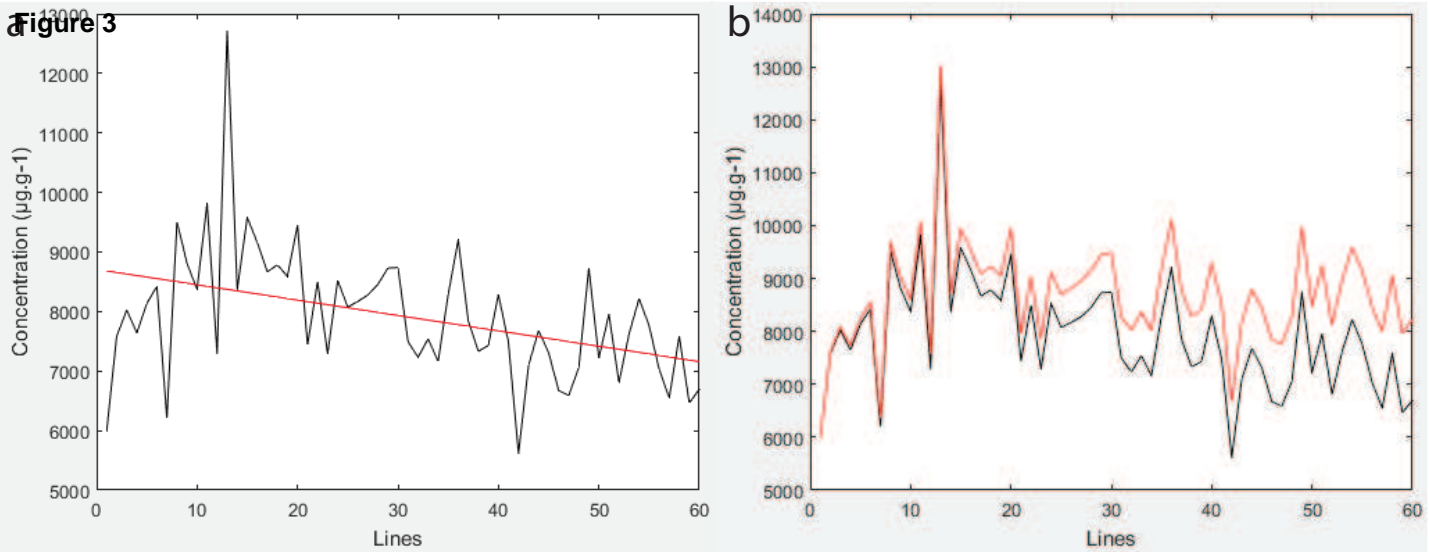




**Figure 4**  
[Click here to download high resolution image](#)

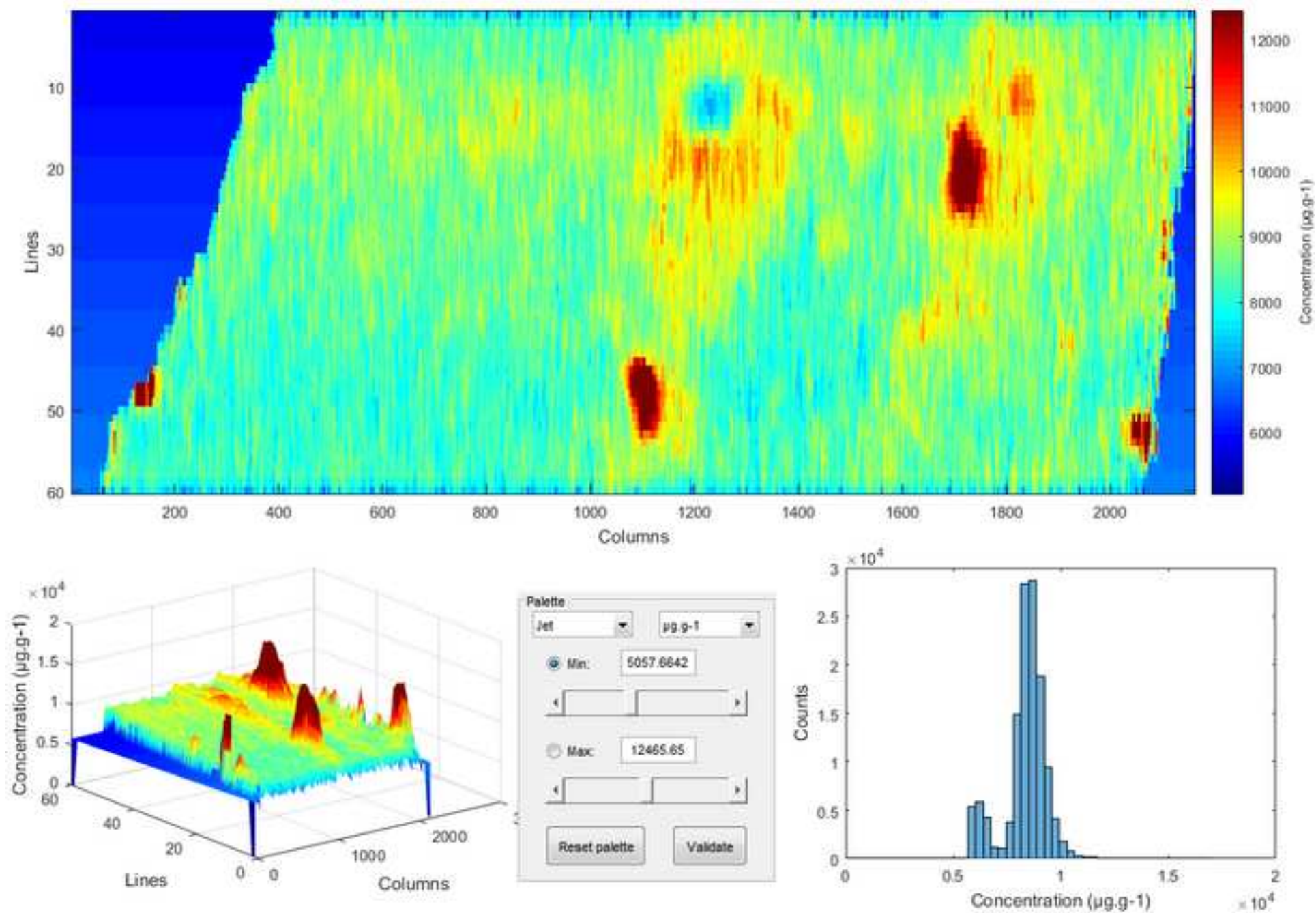


Figure 5

Pre-AERYN

Post-AERYN

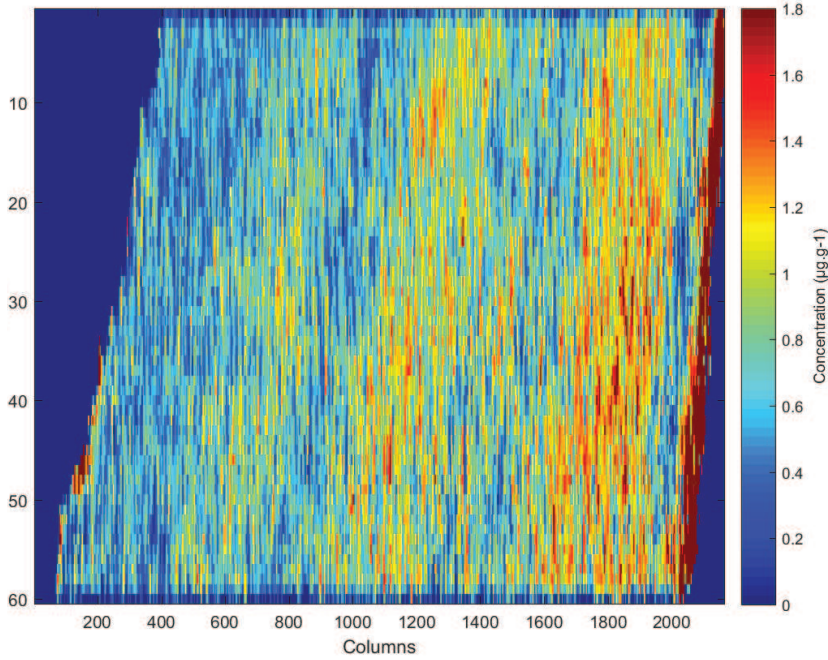
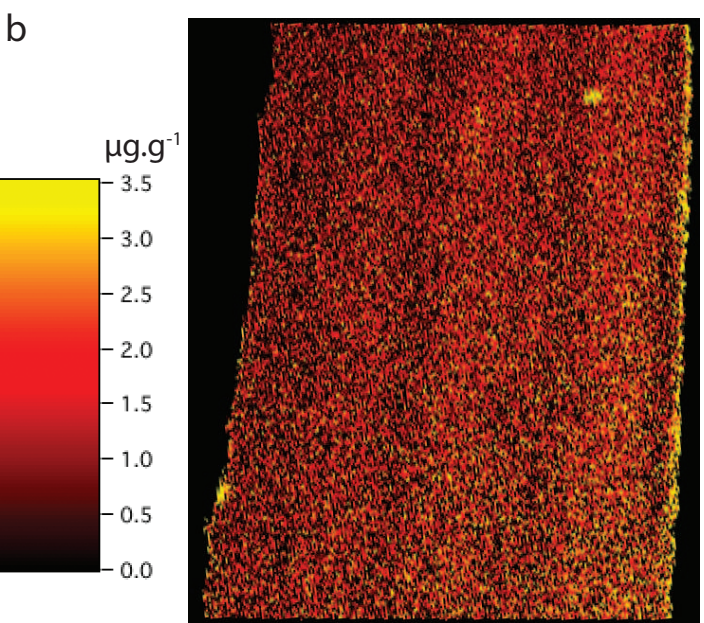
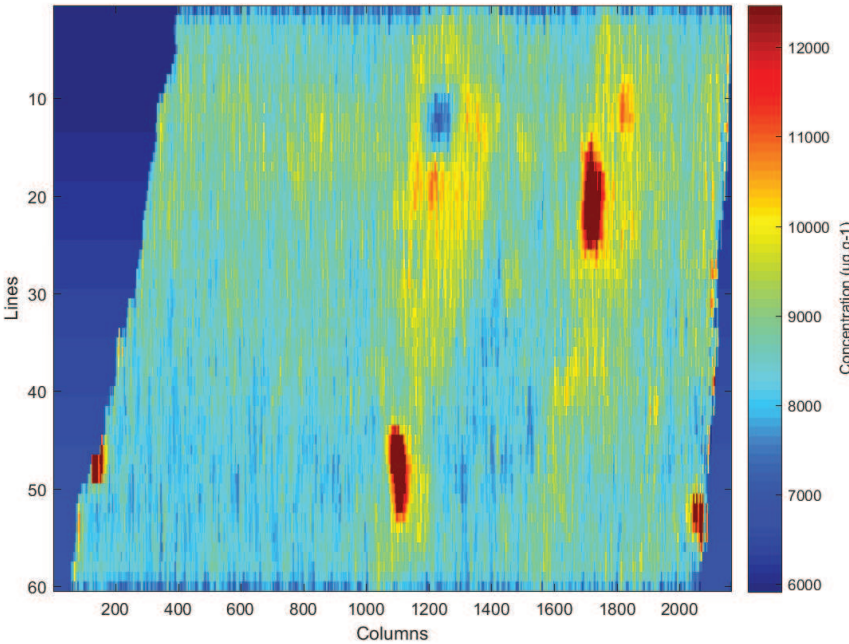
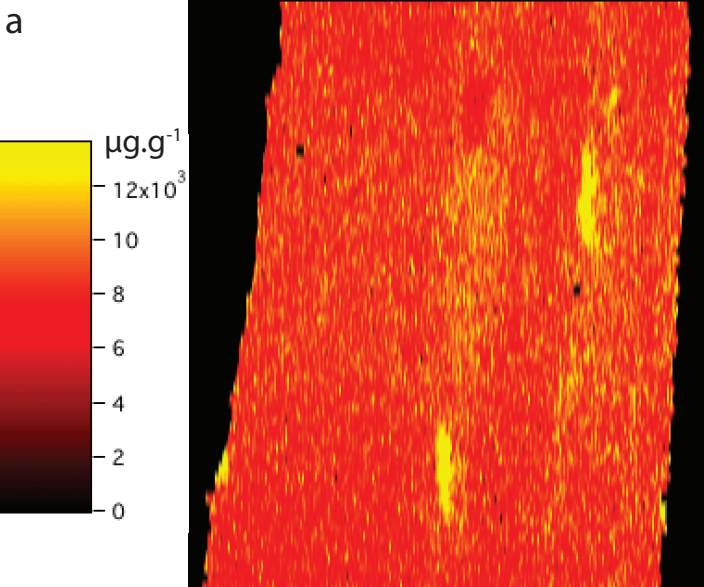
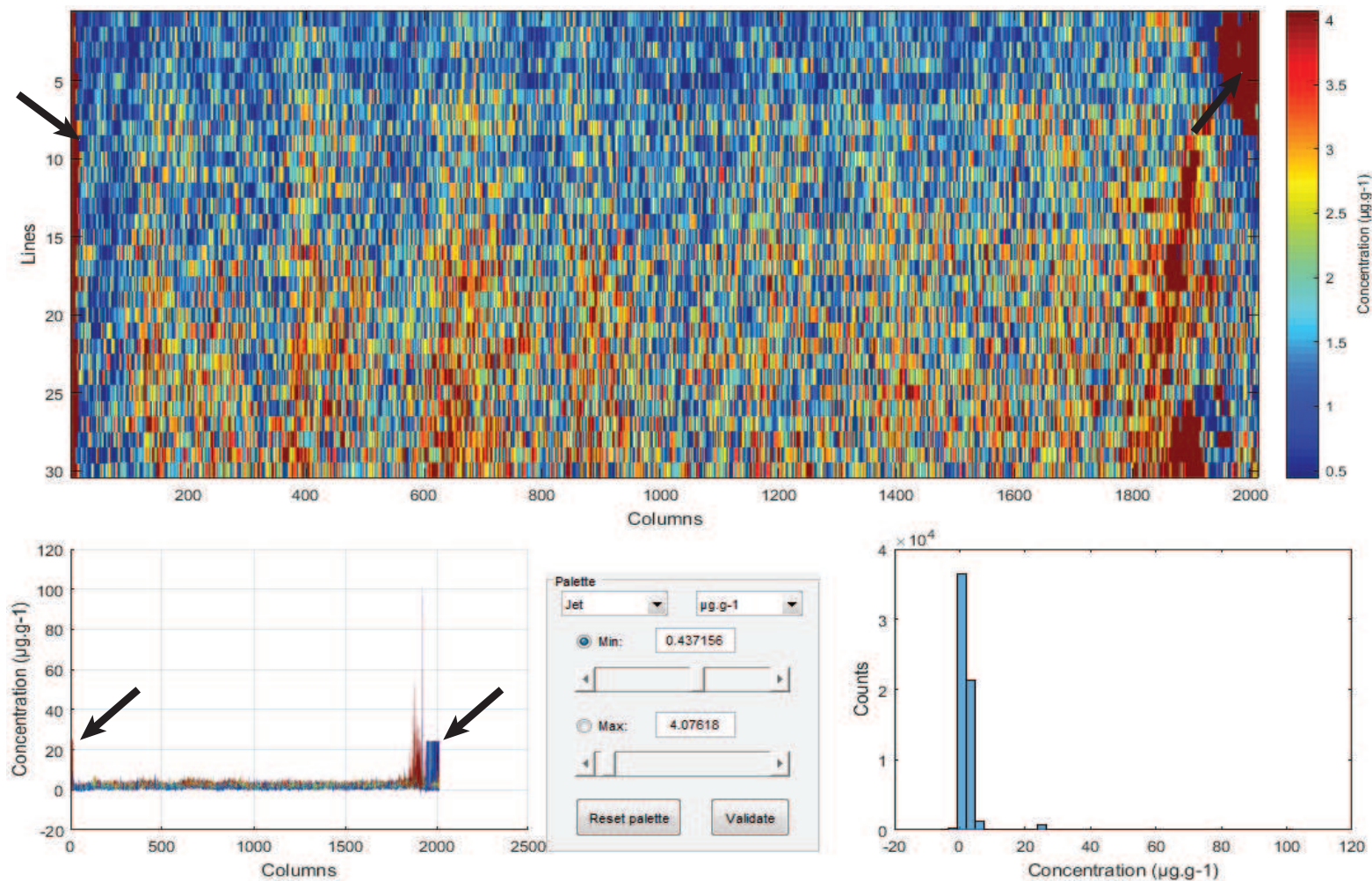




Figure 6

a



b

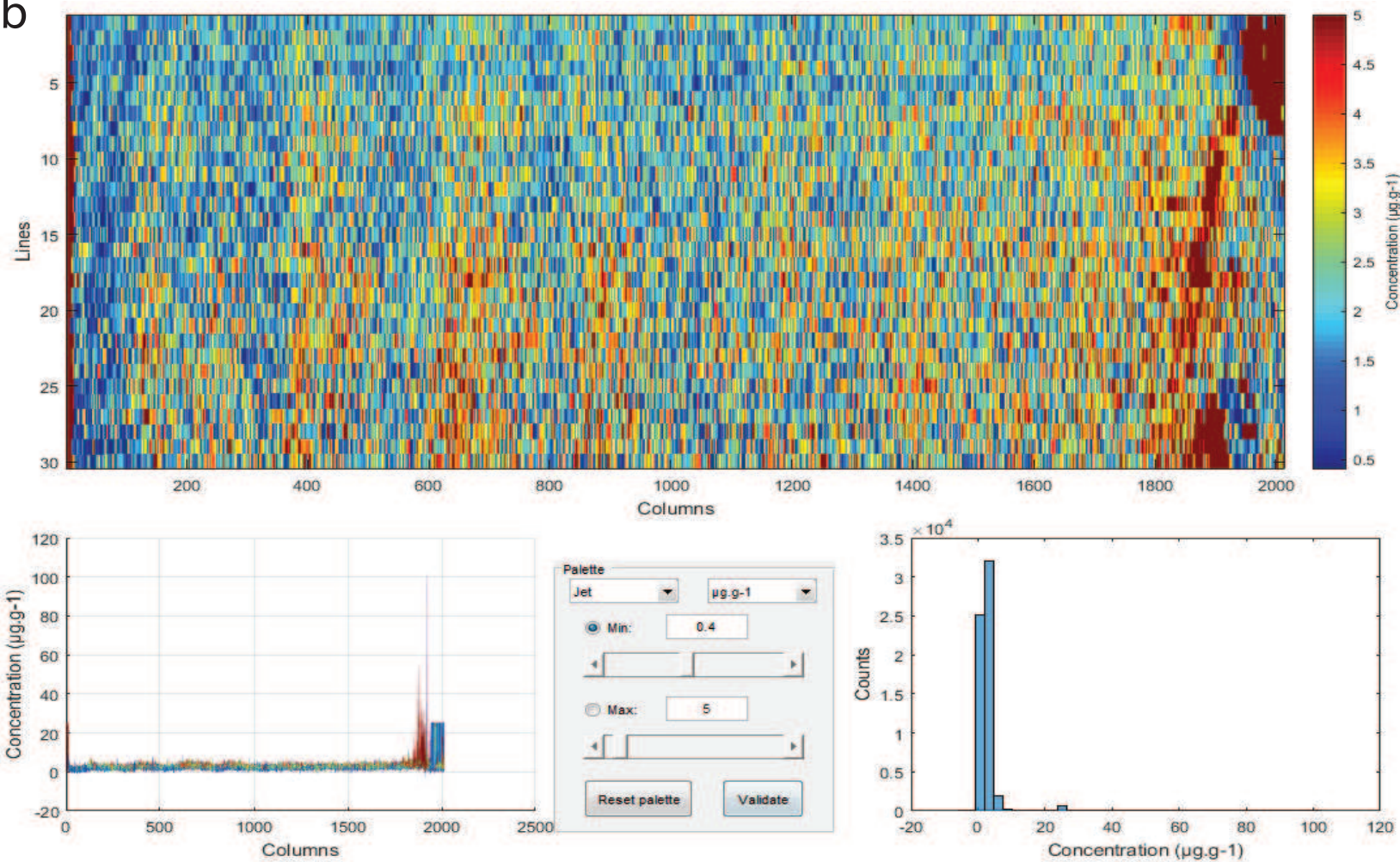




Figure 7

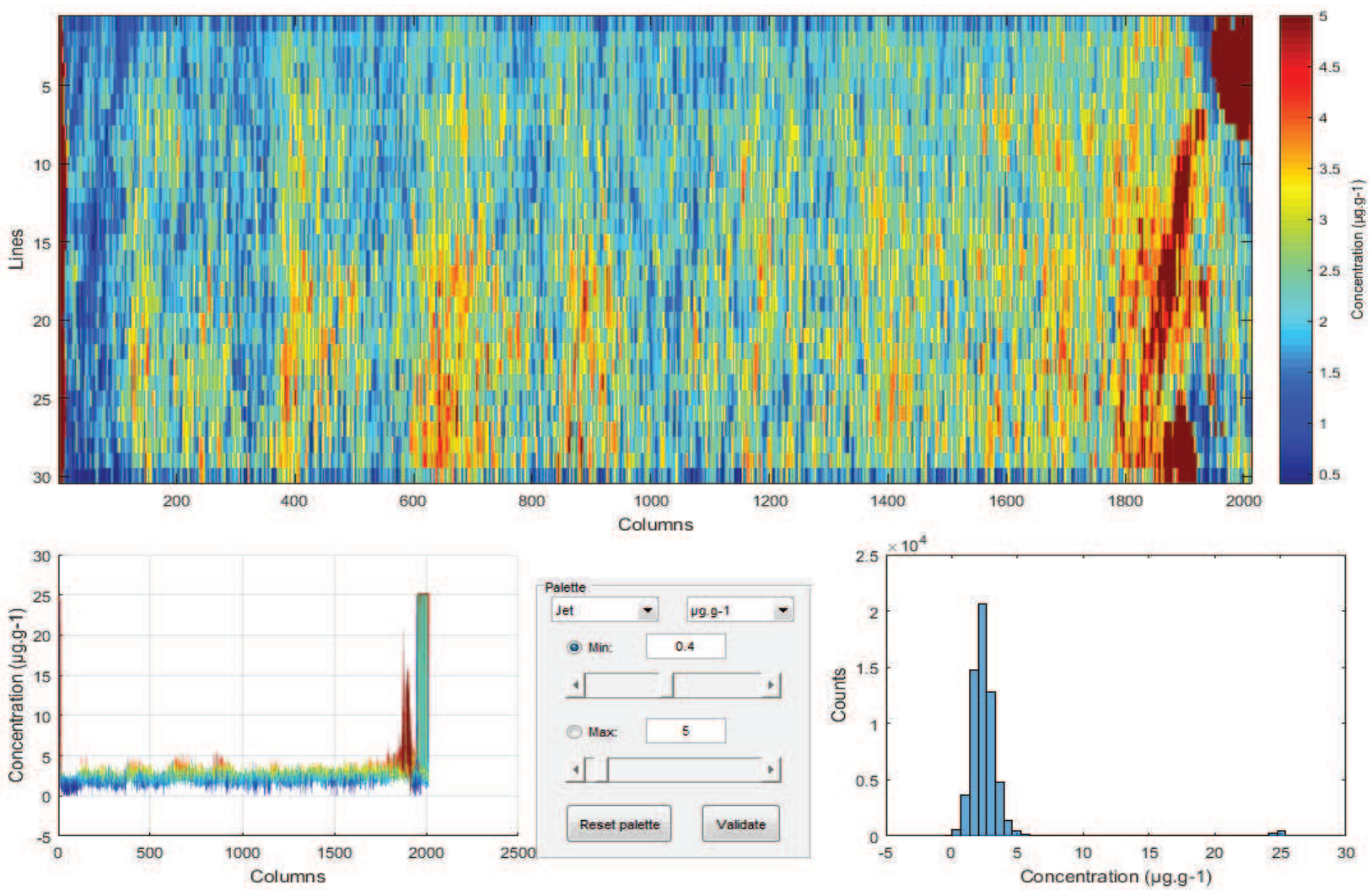
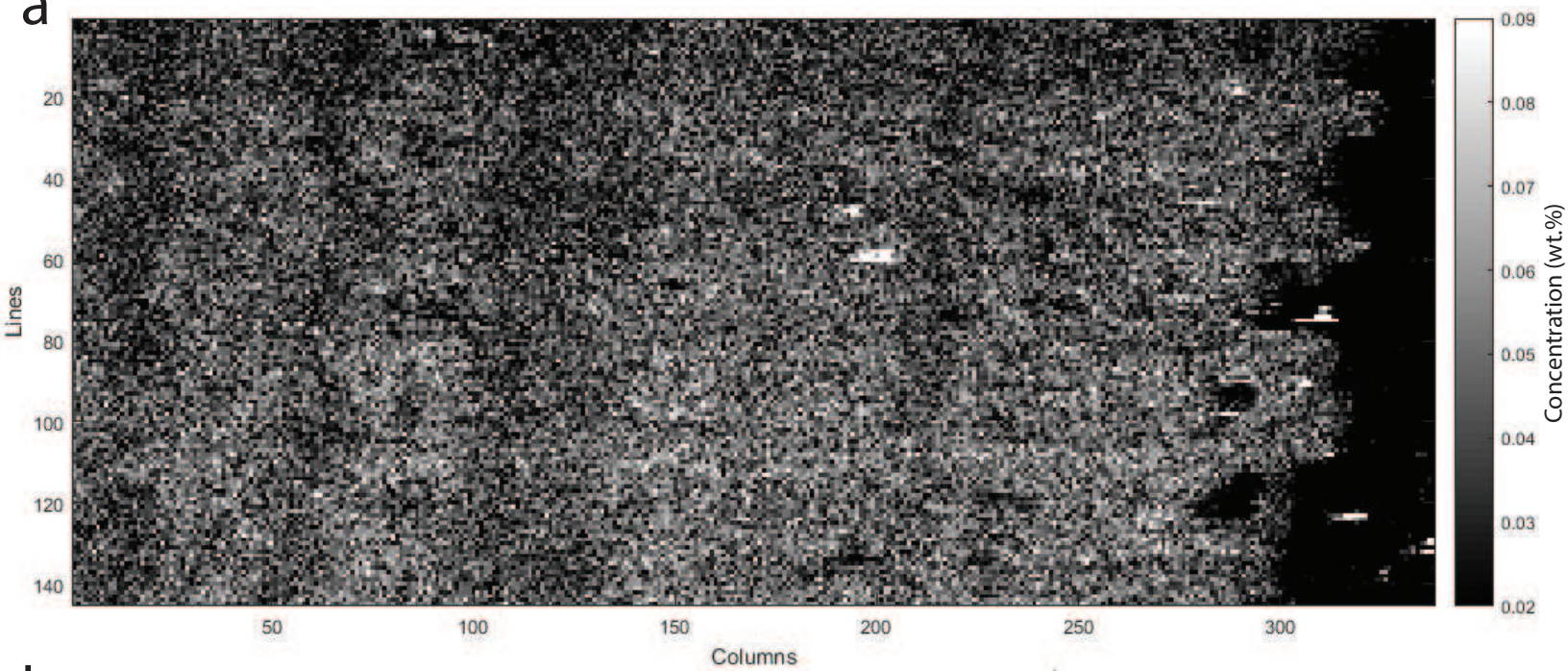


Figure 8

a



b

